

# Chapter 6

## Identification of Soil-Structure Systems



S. Farid Ghahari, Fariba Abazarsa and Ertugrul Taciroglu

**Abstract** Structures interact with soil under seismic excitations through both inertial and kinematic effects. These soil-structure interaction (SSI) effects are often significant and system identification methods can be used to characterize and quantify them. However, system identification of soil-structure systems is fraught with difficulties. SSI renders it virtually impossible to directly measure the earthquake input motions for a soil-structure system due to kinematic interaction effects, which is the term used for denoting the differences between the soil motions at the free field and the foundation, in the absence of superstructure mass. Moreover, because of disproportional distribution of damping in a soil-structure system, normal modes are no longer able to decompose the overall system's equations of motion. Additionally, while some structures may remain linearly elastic even under high levels of vibration, soil behaves nonlinearly even under weak ground motions. Through work spanning the past decade various new methods of system identification have been devised appropriate for soil-structure systems—some of which, incidentally, are by the authors of the present article. This chapter provides an overview of the said techniques along with several application examples.

**Keywords** Soil-structure interaction · Blind identification · Output-only identification · Response data

### 6.1 Introduction

Soil-Structure Interaction (SSI) has been well studied for more than 40 years (e.g., [1–3]). SSI can be classified into two distinct effects—namely, *kinematic* and *inertial* [4]. Even in the absence of a superstructure, a massless foundation experiences different movement during an earthquake—called the Foundation Input Motion (FIM)—from the Free-Field Motion (FFM), which would have been recorded at

---

S. F. Ghahari · F. Abazarsa · E. Taciroglu (✉)  
Civil & Environmental Engineering Department, University  
of California, Los Angeles, CA 90095, USA  
e-mail: [etacir@ucla.edu](mailto:etacir@ucla.edu)

© Springer Nature Switzerland AG 2019  
M. P. Limongelli and M. Çelebi (eds.), *Seismic Structural Health Monitoring*, Springer  
Tracts in Civil Engineering, [https://doi.org/10.1007/978-3-030-13976-6\\_6](https://doi.org/10.1007/978-3-030-13976-6_6)

139

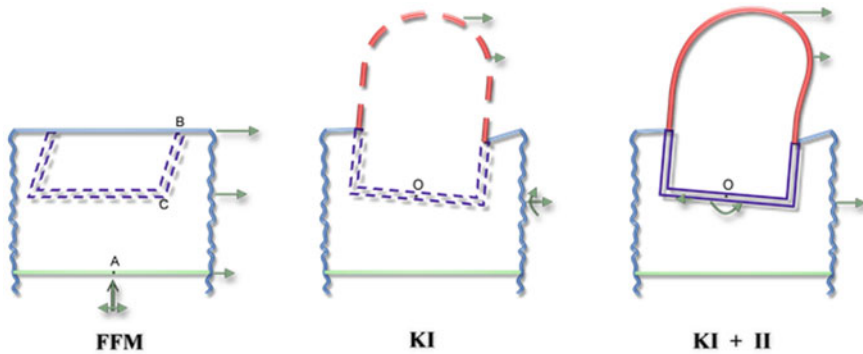


**Fig. 6.1** Soil-foundation-structure interaction (courtesy of Mojtaba Mahsuli)

the same site if the foundation was not there (see Fig. 6.1 left and middle). This effect is termed as the Kinematic Interaction (KI), and is due to the stiffness differences between the foundation and its surrounding soil. FIM is dependent on both the foundation and soil properties, and the wave fields. For example, “base-slab averaging” is a major source of KI in surface foundation systems where the foundation slab experiences an average of inclined and incoherent waves [5–7]. For embedded and piled foundations, base-slab averaging is accompanied with embedment effects, which renders FIM to be further different from FFM [8–11]. Dynamic response of the structure inserts force and moments to the base and causes the foundation to have a different response from FIM. This effect is referred to as Inertial Interaction (II) (Fig. 6.1 right). Due to its inertia, the vibrating structure effectively acts as a wave propagating source and alters the wave field around it. Consequently, motions recorded around/near the structure cannot be assumed as the free-field even if KI effects are negligible.

One approach to analyze SFSI effects is to create and analyze a complete Finite Element (FE) model of the full system wherein the soil medium is represented as a semi-infinite domain (see, for example, [12]). In this method of analysis, which is usually referred to as the “direct method,” the region of the soil containing the structure is modeled up to an artificial boundary where special provisions are made in order to avoid reflections of the outbound waves (see, for example, [13]). Because superposition is not required, material nonlinearities in both the soil domain and the structure can be considered; thus, this is a quite general approach to SSI analysis. Nevertheless, the direct method is typically avoided in engineering practice due to the labor-intensive finite element model development, and the high computational cost associated with carrying out successive simulations under multiple input motions. The primary alternative approach is the so-called “substructure method,” wherein the SSI problem is broken down into three distinct parts, which are combined to formulate the complete solution as follows: (i) estimation of FIMs (Fig. 6.2a), (ii) determination of soil-foundation Impedance Functions (IFs) (Fig. 6.2b), and (iii)

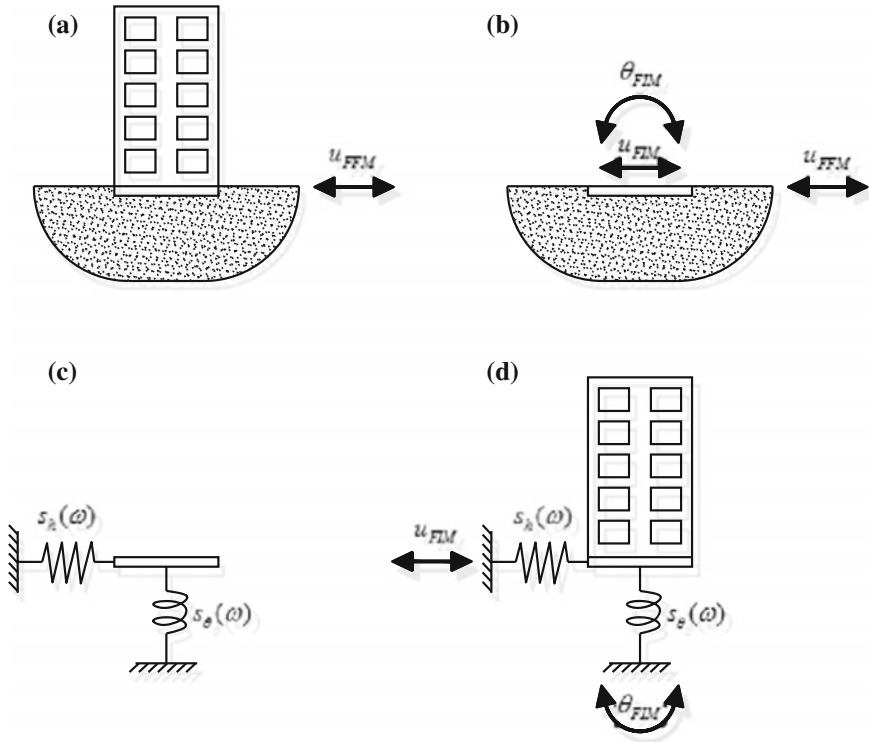


**Fig. 6.2** A schematic presentation of the substructure method: **a** soil-structure response problem, **b** evaluation of FIMs, **c** evaluation of impedance function, and **d** analysis of structure on compliant base subjected to FIMs [22]

dynamic analysis of the structure supported on a compliant base represented by the IF and subjected to the FIMs (Fig. 6.2c).

System Identification (SI) is at the heart of Structural Health Monitoring (SHM). Seismic Structural Health Monitoring (S<sup>2</sup>HM) is more challenging, because traditional Operational Modal Analysis (OMA) techniques (e.g., [14–16]) cannot be used for seismic signals, as they assume various statistical properties on signals, which are not valid for earthquake excitations (see, for example, [17]).

According to the substructure method described above, S<sup>2</sup>HM becomes even more challenging for SSI systems, because FFMs cannot be used as input excitations anymore, and FIMs are physically unmeasurable. Therefore, Input-Output (IO) identification methods (e.g., [18]) are no longer applicable. Moreover, the IFs are frequency- and amplitude-dependent (see, for example, [19, 20]). IFs also have a (radiation) damping term, which renders the mode shapes of the overall dynamic system complex-valued [21]. Through work spanning the past decade—by the authors, their collaborators and as well as other colleagues—various new methods of system identification have been devised that can handle soil-structure systems. In what

**Table 6.1** Input-output pairs for identifying modal properties associated with different conditions of base fixity [28]

System	Input	Output
Flexible base	$u_g$	$u_g + u_f + h\theta + u$
Pseudo-flexible base	$u_g + u_f$	$u_g + u_f + h\theta + u$
Fixed base	$u_g + u_f + h\theta$	$u_g + u_f + h\theta + u$

follows, the said techniques are reviewed and several application examples are provided.

## 6.2 Identification of SSI Systems

One of the first well-instrumented structures is the Millikan Library, for which SSI effects were incidentally observed to be quite important. As such, research efforts on identification of soil-foundation systems from their seismic responses (e.g., [23]) are almost contemporary with system identification of buildings (e.g., [24]). A full history of identification studies on this well-known building can be found in [25]. However, the studies initiated by Luco [26] and Safak [27] and later continued by Stewart and Fenves [28] and Safak [29] on identifying and quantifying SSI effects are generally deemed as the pioneering works in this field. They mathematically showed that depending to the type of input motion used in an Input-Output (IO) identification strategy, various idealizations of a soil-structure-foundation system could be identified as presented in Table 6.1. According to their definitions, the “flexible base” system could be identified if KI is negligible and FFM ( $u_g$ ) is used as input excitation. Otherwise, using various combinations of signals recorded at the foundation ( $u_f$ : sway and/or  $\theta$ : rocking) will result in the identification of systems with fictitious boundary conditions called “pseudo-flexible base” or “fixed base” systems. It is obvious that KI could be present in many cases. Also, the motions recorded close to the buildings could be affected by the waves emitted from the vibrating building—which, in fact, can be detected in the results presented by [28, 30]. Therefore, utilization of IO techniques for identifying soil-foundation-structure systems is rife with potential errors.

### 6.2.1 Blind Modal Identification (BMID) Techniques

#### 6.2.1.1 Theoretical Background

Because of the unavailability of true input motions that can be used to identify flexible base systems using IO methods, and due to the inherent limitation of classic

Output-Only (OO) identification techniques, Ghahari et al. [31] developed a new OO identification method based on a class of Blind Source Separation (BSS) techniques [32], which can be used for non-stationary seismic data. This method takes advantage of the non-stationarity of seismic signals, indeed, and is based on the assumption that there are points in the time-frequency plane where the modes are disjoint. The details of the method are briefly reviewed next.

The governing equations of motion for a Multi-Degree-Of-Freedom (MDOF) system with  $n_d$  DOFs, which is excited by a unidirectional (scalar) FIM, can be expressed as follows

$$\mathbf{M}\ddot{\mathbf{x}}(t) + \mathbf{C}\dot{\mathbf{x}}(t) + \mathbf{K}\mathbf{x}(t) = -\mathbf{M}\mathbf{I}\ddot{x}_g(t) \quad (6.1)$$

where  $\mathbf{M}$ ,  $\mathbf{C}$ , and  $\mathbf{K}$  are the constant  $n_d \times n_d$  mass, damping, and stiffness matrices of the system, respectively. The vector  $\mathbf{x}(t)$  contains relative displacement responses of the system at all DOFs;  $\ddot{x}_g(t)$  is a scalar time-signal, which represents the (unknown) FIM; and  $\mathbf{I}$  is the influence vector [33]. In practical cases, the absolute acceleration of the structure is recorded, which is

$$\ddot{\mathbf{x}}^t(t) = \ddot{\mathbf{x}}(t) + \mathbf{I}\ddot{x}_g(t). \quad (6.2)$$

By assuming a proportional damping matrix, the absolute acceleration response can be expressed in modal space as

$$\ddot{\mathbf{x}}^t(t) = \Phi\ddot{\mathbf{q}}(t) \quad (6.3)$$

where  $\Phi$  is an  $n_d \times n_d$  real-valued mode shape matrix whose  $i$ -th column ( $\phi_i$ ) is the  $i$ -th mode shape; and  $\ddot{\mathbf{q}}(t)$  is a vector that contains the absolute acceleration modal coordinates.

The Cohen-class Spatial Time-Frequency Distribution (STFD) [34] of responses can be calculated as

$$\mathbf{D}_{\ddot{\mathbf{x}}^t\ddot{\mathbf{x}}^t}(t, f) = \int_{-\infty}^{+\infty} h(\tau) \int_{-\infty}^{+\infty} g(s-t) \mathbf{z}\left(s + \frac{\tau}{2}\right) \mathbf{z}^H\left(s - \frac{\tau}{2}\right) ds e^{-2\pi j f \tau} d\tau \quad (6.4)$$

where  $\mathbf{z}(t)$  is the analytic associate of  $\ddot{\mathbf{x}}^t(t)$ , and the functions  $h$  and  $g$  are smoothing functions that reduce the spurious inference terms [35]. The superscript  $H$  denotes a Hermitian transpose. This specific time-frequency distribution is called the smoothed pseudo Wigner-Ville distribution, which is available through a MATLAB [36] toolbox freely available at <http://tftb.nongnu.org/> [37]. Calculating the STFD of both sides of Eq. (6.3) yields

$$\mathbf{D}_{\ddot{\mathbf{x}}^t\ddot{\mathbf{x}}^t}(t, f) = \Phi \mathbf{D}_{\ddot{\mathbf{q}}\ddot{\mathbf{q}}}(t, f) \Phi^T \quad (6.5)$$

Considering the STFD definition provided in Eq. (6.4), and by assuming that it is an ideal time-frequency distribution tool by which the interference-terms are not produced, the Time-Frequency (TF) points can now be classified into three different groups based on the localization of modal coordinates observed in earthquake engineering:

- **Single Auto-Term TF Point (SATFP):** At these points, only one mode is present; thus,  $\mathbf{D}_{\ddot{q}\ddot{q}}(t, f)$  matrices are diagonal with only one non-zero diagonal element.
- **Multiple Auto-Term TF Point (MATFP):** At these points, several modes are present; thus,  $\mathbf{D}_{\ddot{q}\ddot{q}}(t, f)$  matrices have non-zero diagonal and off-diagonal elements.
- **Cross-Term TF Point (CTTFP):** At these points, the cross-TFDs of modal coordinates are non-zero, while their corresponding auto-TFDs are zero. Thus,  $\mathbf{D}_{\ddot{q}\ddot{q}}(t, f)$  matrices are off-diagonal.

As will be discussed in subsequent subsections, SATFPs play an important role in the BMID techniques. While there are various procedures to find these points from  $\mathbf{D}_{\ddot{x}\ddot{x}'}(t, f)$  matrices, the proper formula and consequently identification procedure are dependent on the number of available measurements/sensors and the number of contributing modes.

### 6.2.1.2 Over-determined Case

Let's assume that the number of active modes ( $n_m$ ) is smaller than the number of sensors ( $n_r$ )—i.e.,  $n_m \leq n_r \leq n_d$ . This case is dubbed the over-determined case. For a moment let us assume that we know the SATFPs corresponding to the  $i$ -th mode, so we have

$$\mathbf{D}_{\ddot{x}\ddot{x}'}(t_i, f_i) = \boldsymbol{\phi}_i D_{\ddot{q}_i\ddot{q}_i}(t_i, f_i) \boldsymbol{\phi}_i^H \quad (6.6)$$

where  $D_{\ddot{q}_i\ddot{q}_i}(t_i, f_i)$  is  $i$ -th mode's auto-TFD and the  $i$ -th diagonal element of  $\mathbf{D}_{\ddot{q}\ddot{q}}(t, f)$ . Equation (6.6) shows that an Eigenvalue Decomposition (EVD) can be used to extract  $\boldsymbol{\phi}_i$  and  $D_{\ddot{q}_i\ddot{q}_i}(t_i, f_i)$  from  $\mathbf{D}_{\ddot{x}\ddot{x}'}(t_i, f_i)$ . However,  $\mathbf{D}_{\ddot{q}\ddot{q}}(t_i, f_i)$  is rank-deficient, and thus,  $\boldsymbol{\Phi}$  can't be uniquely determined. Moreover, external criteria are needed to specify the true auto-terms of each source signal and to decide which mode's auto-term should be used for EVD. The difference between the number of modes and the number of sensors poses further difficulties for EVD. Belouchrani and Amin [32] showed that it is necessary and sufficient to use all of the auto-terms simultaneously, without knowing to which source they belong. Hence, a Joint Approximate Diagonalization (JAD) technique is employed instead of EVD [38].

Because the JAD algorithm is restricted to finding a unitary diagonalizing matrix, a preprocessing step called whitening  $\ddot{\mathbf{x}}'(t) = \mathbf{W}\ddot{\mathbf{x}}'(t)$  is carried out where the whitening matrix is obtained from the correlation matrix of  $\ddot{\mathbf{x}}'(t)$  at zero lag. The whitening process reduces the determination of the  $n_r \times n_m$  mode shape matrix  $\boldsymbol{\Phi}$  to that of a unitary  $n_m \times n_m$  matrix  $\mathbf{U}$ , that is

$$\mathbf{D}_{\ddot{\mathbf{x}}\ddot{\mathbf{x}}'}(t, f) = \mathbf{U}\mathbf{D}_{\ddot{\mathbf{q}}\ddot{\mathbf{q}}}(t, f)\mathbf{U}^H. \quad (6.7)$$

Now, any whitened STFD-matrix is diagonal when stated in the basis of the columns of the matrix  $\mathbf{U}$ . As mentioned previously, this unknown unitary matrix can be identified through a Joint Approximate Diagonalization of  $\mathbf{D}_{\ddot{\mathbf{x}}\ddot{\mathbf{x}}'}(t, f)$  at the SATFPs. After the identification of  $\mathbf{U}$ , the mode shape matrix, and the modal coordinates  $\ddot{\mathbf{q}}(t)$ , may be recovered as follows

$$\Phi = \mathbf{W}^\# \mathbf{U}, \quad (6.8)$$

$$\ddot{\mathbf{q}}(t) = \mathbf{U}^H \mathbf{W} \ddot{\mathbf{x}}'(t) \quad (6.9)$$

where the superscript # denotes a Moore-Penrose pseudo-inverse. Once the modal coordinates are recovered, natural frequencies and damping ratios can be identified by cross-solving for the modal coordinates, as they have the same input excitations and only differ by a factor. Details of this process are omitted here for the sake of brevity and can be found in [31].

There are various criteria that can be used for identifying the SATFPs from  $\mathbf{D}_{\ddot{\mathbf{x}}\ddot{\mathbf{x}}'}(t, f)$ . However, at each SATFP, each STFD matrix is of rank one—or at least, each matrix has one significantly large eigenvalue compared to its other eigenvalues. Therefore, the following criterion may be used to deselect the Non-SATFPs [39],

$$\left| \frac{\lambda_{max}[\mathbf{D}_{\ddot{\mathbf{x}}\ddot{\mathbf{x}}'}(t, f)]}{\|\mathbf{D}_{\ddot{\mathbf{x}}\ddot{\mathbf{x}}'}(t, f)\|_F} - 1 \right| > \varepsilon \quad (6.10)$$

where  $\|\cdot\|_F$  denotes the Frobenius norm,  $\varepsilon$  is a small positive scalar (typically, 0.001) and  $\lambda_{max}[\cdot]$  represents the largest eigenvalue of its argument matrix. Note that in this new criterion, the STFD matrix of the original data (as opposed to that of the whitened data) is used.

To verify the method, a 5-DOF shear building is placed on top of a sway-rocking foundation. Mass-proportional damping with 10% first mode damping is considered for the entire system. The response of the system is simulated under a horizontal accelerogram recorded in El Centro Array #9 during the Imperial Valley earthquake, 1940. As an illustration, TFD of the roof response is shown in Fig. 6.3a. Figure 6.3b displays the time variation of Modal Assurance Criterion (MAC) values between the identified and exact mode shapes in various 10-second time windows. While the method is very successful, this figure shows how the method is able to take advantage of the non-stationary nature of ground motions to identify Mode 4 in a short time window.

The identified natural frequencies and damping ratios are shown in Table 6.2 along with exact values. As seen, neglecting minor errors in damping ratios which are accepted, the method is very successful.

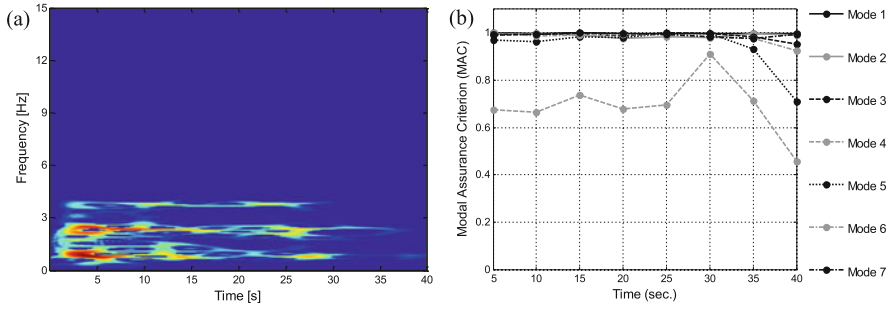


**Fig. 6.3** a TFD of the roof response, and b time variation of MAC index

**Table 6.2** Comparison of the identified and analytical modal properties

	Mode	1	2	3	4	5	6	7
Exact	$f_n$ (Hz)	0.91	2.45	3.87	4.91	5.43	7.57	10.97
	$\xi$ (%)	10.00	3.70	2.34	1.85	1.67	1.20	0.83
Identified	$f_n$ (Hz)	0.90	2.43	3.86	4.81	5.30	7.59	10.96
	$\xi$ (%)	8.02	3.76	2.29	1.83	1.59	1.21	0.83

**6.2.1.3 Torsionally Coupled Buildings**

The method presented in the last section can be easily extended to buildings that exhibit lateral-torsional coupling [40] because modal superposition is still valid. However, the identification of natural frequencies and damping ratios from the recovered modal coordinates is more challenging than the unidirectional case. In [40] it was shown that if we use the cross-relation between close modes, we are able to identify modal properties with acceptable accuracy.

To examine the performance of this method, we applied it to the earthquake data recorded at the three-story Hilltop Medical building (CSMIP Station No. 58506) during the 1989 Loma Prieta earthquake. The building’s instrumentation layout is shown in Fig. 6.4. While the building has a symmetrical plan, its torsional movements have been reported in the literature [41]. Here, we apply our identification technique to the first 40 s of the recorded responses of the 2nd, 3rd, and roof floors (ground floor response signals are excluded due to low levels of motion). Table 6.3 displays the identified natural frequencies and damping ratios versus those identified from similar data sets using a completely different method [42]. While we do not expect to see identical results, they are quite similar.

**6.2.1.4 Multiple Support Excitation**

Along the path towards more complex problems, the BMID method was extended to the analysis of bridge structures under multiple support excitations [43]. Again,



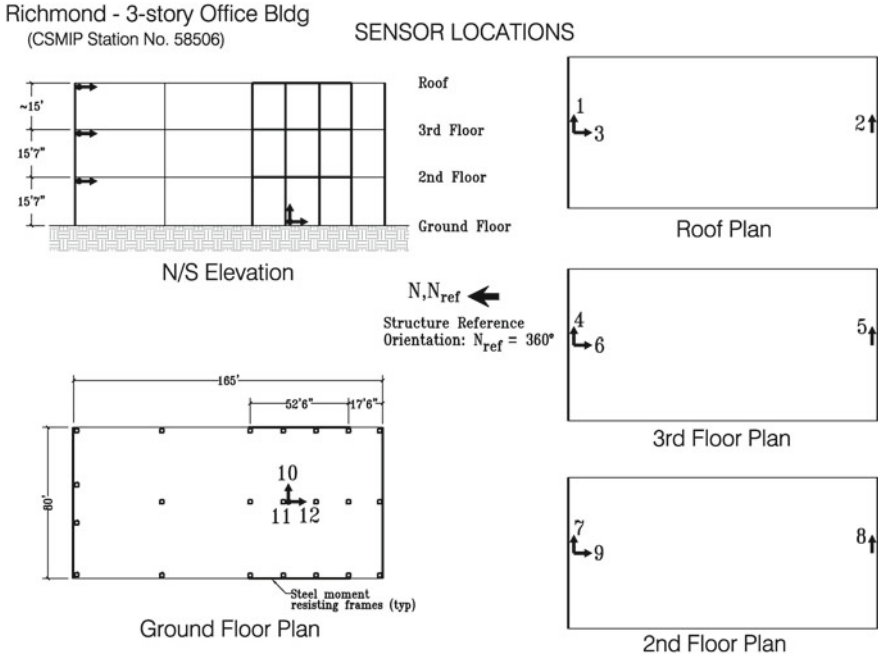


**Fig. 6.4** Instrumentation layout of CSMIP station 58506

**Table 6.3** Comparison between identified natural frequencies and damping ratios with others' results

	Mode	1	2	3	4	5	6
Exact	$f_n$ (Hz)	1.35	1.64	2.27	3.76	4.75	5.58
	$\xi$ (%)	8.4	4.8	1.4	4.8	5.3	–
[42]	$f_n$ (Hz)	1.30	1.61	2.22	3.83	4.61	5.38
	$\xi$ (%)	8.4	4.5	4.6	7.2	6.2	7.9

the first step—i.e., modal decomposition—is not affected by this extension, but the identification of natural frequencies and damping ratios is a challenging task.

Let's assume that the modal coordinates (in the absolute acceleration sense) are already identified. The  $i$ -th modal coordinate can be written as a superposition of  $i$ -th modal coordinates under each support excitation,  $\ddot{q}_i^t[k] = \sum_{l=1}^{n_g} \ddot{q}_i^{t,l}[k]$ , where  $n_g$  is the number of support excitations and

$$\ddot{q}_i^{t,l}[k] = A_i \ddot{q}_i^{t,l}[k - 1] + B_i \ddot{q}_i^{t,l}[k - 2] + \beta_i^l C_i \ddot{x}_{gl}[k] + \beta_i^l D_i \ddot{x}_{gl}[k - 1] \quad (6.11)$$

where

$$A_i = 2e^{-\xi_i \omega_{ni} \Delta t} \cos(\omega_{di} \Delta t), \quad (6.12)$$

$$B_i = -e^{-2\xi_i \omega_{ni} \Delta t}, \quad (6.13)$$

$$C_i = 2\xi_i \omega_{ni} \Delta t, \quad (6.14)$$

$$D_i = \omega_{ni} \Delta t e^{-\xi_i \omega_{ni} T} \left[ \frac{\omega_{ni}}{\omega_{di}} (1 - 2\xi_i^2) \sin(\omega_{di} \Delta t) - 2\xi_i \cos(\omega_{di} \Delta t) \right], \quad (6.15)$$

where  $\Delta t$  is sampling time; and  $\xi_i$ ,  $\omega_{ni}$ , and  $\omega_{di} = \omega_{ni} \sqrt{1 - \xi_i^2}$  respectively denote the damping ratio, and the undamped and damped natural frequencies of the  $i$ -th mode. We can determine the unknown parameters  $\mathbf{x} = [\xi_1, \dots, \xi_n, \omega_{n1}, \dots, \omega_{nn}, \beta_1^1, \dots, \beta_n^1, \dots, \beta_n^{n_g}, \ddot{x}_{g1}, \dots, \ddot{x}_{gn_g}]$  by solving the following minimization problem

$$\min_{\mathbf{x}} \|\mathbf{G}(\mathbf{x})\|_2^2 \quad (6.16)$$

where  $\mathbf{G}(\mathbf{x})$  is the difference between the recovered modal coordinates and their counterparts calculated using Eq. (6.11) for all times and modes stacked in a single vector. As long as the number of equations ( $N \times n_m$ ) is greater than the number of unknowns ( $n_m + n_m + n_g \times n_m + n_g \times N$ ), the optimization problem will have a solution, but it will be highly non-convex. Based on this reason, we limit our cases to the those in which the input motions experienced by the bridge supports differ only by a time delay.

For validation, the proposed approach was applied to experimental data collected on a 1:50 scale bridge shown in Fig. 6.5 [44]. To excite the test model, an artificially generated time-history displacement was used. For considering the wave passage effects, the input motion was applied with a 7 ms phase-delay at each pier from left to right (there are 5 piers) and the response was recorded at the three middle masses. The identified input excitation is compared with the exact one applied in Fig. 6.6a. As seen, they are very close to each other. To obtain the phase delay, we carried out optimization for a range of delays and determined the one that yields the minimum residual norm, which is shown in Fig. 6.6b. The values of this optimal phase delay is around the 7 ms used by Norman and Crewe.

### 6.2.1.5 Under-determined Case

As mentioned earlier, the main assumption in BMID is that the number of modes is smaller than the number of measured responses. In this section, we extend the method to the so-called under-determined cases, for which  $n_m \geq n_r$  [45].

The first change takes place in the SATFP selection step. We replace EVD with Singular Value Decomposition (SVD) and select points for which the following metric is very close to 1 [46]

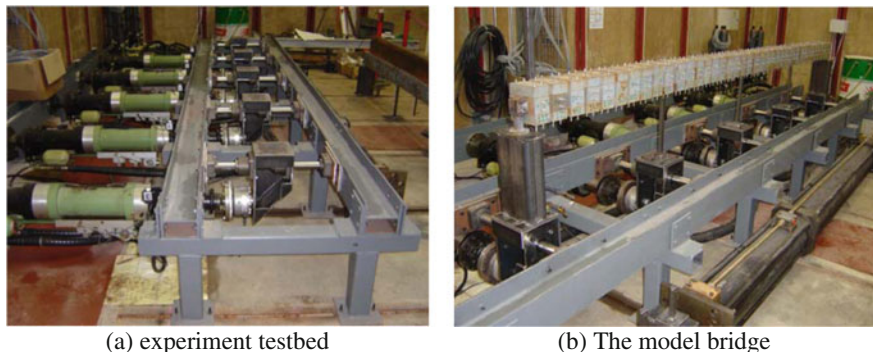


Fig. 6.5 The scaled bridge model under test

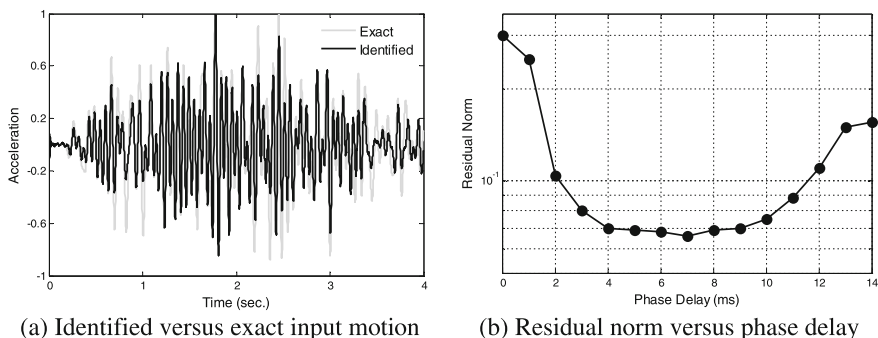


Fig. 6.6 Identification results

$$C(t, f) = \frac{\max_i \{\sigma_i [\mathbf{D}_{\ddot{x}'\ddot{x}'}(t, f)]\}}{\sum_i \{\sigma_i [\mathbf{D}_{\ddot{x}'\ddot{x}'}(t, f)]\}} \tag{6.17}$$

where  $\sigma_i[\cdot]$  denotes the singular value of its argument matrix. Now, suppose that there are two SATFPs  $(t_1, f_1)$  and  $(t_2, f_2)$  that are related to  $k$ -th mode. We would then have,

$$\mathbf{D}_{\ddot{x}'\ddot{x}'}(t_1, f_1) = \phi_k D_{\ddot{q}_k \ddot{q}_k}(t_1, f_1) \phi_k^T, \tag{6.18}$$

$$\mathbf{D}_{\ddot{x}'\ddot{x}'}(t_2, f_2) = \phi_k D_{\ddot{q}_k \ddot{q}_k}(t_2, f_2) \phi_k^T. \tag{6.19}$$

As seen,  $\mathbf{D}_{\ddot{x}'\ddot{x}'}(t_1, f_1)$  and  $\mathbf{D}_{\ddot{x}'\ddot{x}'}(t_2, f_2)$  have the same eigenvectors (corresponding to the largest eigenvalue). That is, the STFD matrices of response signals at all SATFPs corresponding to the same mode have the same eigenvector. Therefore, a clustering approach can be used to categorize the principal eigenvectors of the STFD matrices of the response signals at all SATFPs into  $n_m$  groups. For this a “ $k$ -means” clustering can be used. This clustering is a partitioning method through which data

(here, a set of eigenvectors) are grouped into  $k$  mutually exclusive clusters. To do so, a distance measure, here MAC, is used and the  $k$ -means approach partitions the eigenvectors into clusters in which the vectors within each cluster are both as close to each other as possible *and* as far from those vectors that belong to other clusters as possible.

Once the mode shapes are identified, modal coordinates' TFDs are recovered through the following approach—as mode shape inversion does not work for the under-determined cases.

Assume that there exists a point  $(t', f')$  at which  $p$  modes are present where  $p < n_m$ . If these  $p$  modes are labeled with indices  $\alpha_1, \alpha_2, \dots, \alpha_p$ , then Eq. (6.5) can be rewritten at this time-frequency point as

$$\mathbf{D}_{\tilde{\mathbf{x}}\tilde{\mathbf{x}}'}(t', f') = \tilde{\Phi} \mathbf{D}_{\tilde{\mathbf{q}}\tilde{\mathbf{q}}}(t', f') \tilde{\Phi}^T \quad (6.20)$$

where

$$\tilde{\Phi} = [\phi_{\alpha_1}, \dots, \phi_{\alpha_p}], \quad (6.21)$$

$$\tilde{\mathbf{q}}(t) = [\tilde{q}_{\alpha_1}(t), \dots, \tilde{q}_{\alpha_p}(t)]^T. \quad (6.22)$$

Since the matrix  $\mathbf{D}_{\tilde{\mathbf{q}}\tilde{\mathbf{q}}}(t', f')$  is full rank, a projector onto the orthogonal complement of  $\mathbf{D}_{\tilde{\mathbf{x}}\tilde{\mathbf{x}}'}(t', f')$  can be defined as

$$\mathbf{P} = \mathbf{I} - \mathbf{V}\mathbf{V}^T \quad (6.23)$$

where  $\mathbf{I}$  is an  $n_r \times n_r$  identity matrix, and  $\mathbf{V}$  is an  $n_r \times p$  matrix formed by the  $p$  principal singular vectors of  $\mathbf{D}_{\tilde{\mathbf{x}}\tilde{\mathbf{x}}'}(t', f')$ . It can be shown that [47]

$$\mathbf{P}\phi_i = \mathbf{0} \quad \forall i \in \{\alpha_1, \alpha_2, \dots, \alpha_p\}, \quad (6.24)$$

$$\mathbf{P}\phi_i \neq \mathbf{0} \quad \forall i \notin \{\alpha_1, \alpha_2, \dots, \alpha_p\}. \quad (6.25)$$

Thus, by considering the noise effects and the calculation errors,  $\{\alpha_1, \alpha_2, \dots, \alpha_p\}$  can be obtained as the  $p$  modes that have the smallest  $\|\mathbf{P}\phi_i\|$ . This process can be employed at all time-frequency points to detect their present modes. Then, the modal coordinates' TFDs can be easily recovered as the diagonal elements of the following matrix,

$$\mathbf{D}_{\tilde{\mathbf{q}}\tilde{\mathbf{q}}}(t', f') = \tilde{\Phi}^\# \mathbf{D}_{\tilde{\mathbf{x}}\tilde{\mathbf{x}}'}(t', f') \tilde{\Phi}^{\#T}. \quad (6.26)$$

By recovering the modal coordinates' TFDs, natural frequencies can be identified as those frequencies that have the highest time-marginal energy, and damping ratios can be identified using the free-vibration portion of the TFD.

To demonstrate the performance of the proposed method, we identify the modal properties of a 10-story shear building from its simulated responses under the horizontal accelerogram recorded at the El Centro Array #9 during the 1940 Imperial Valley earthquake. We carry out identification under incomplete instrumentation in which the responses recorded at the 2nd, 4th, 5th, 6th, and 10th stories are used. Figure 6.7 shows the identified mode shapes (green and red) versus the exact (gray) ones. The figure also displays the mode shapes corresponding to all SATFPs in each cluster. Note that the second estimation is obtained by finding the centroid of the clusters after removing elements with low silhouette indices. As seen, the mode shapes are identified very accurately. By using the proposed recovering technique, the modal coordinates' TFDs are also recovered and are displayed in Fig. 6.8 for two modes. The exact TFDs calculated by using the exact modal coordinates are also shown for comparison, showing almost perfect reconstruction.

### 6.2.1.6 Extended BMID

Tensor decomposition is a powerful tool, which recently attracted attention in system identification applications [48]. The authors employed Parallel Factor Decom-

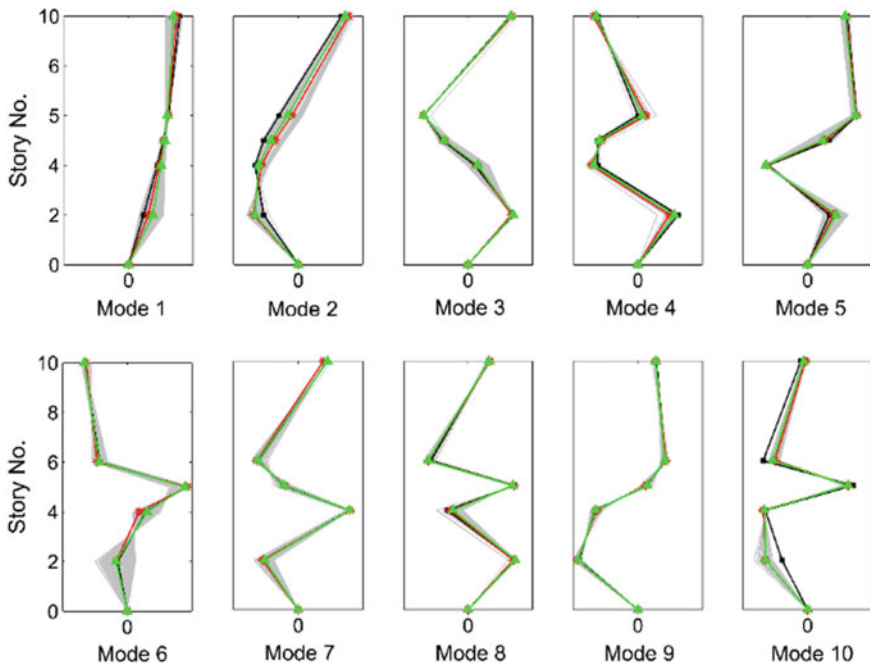


**Fig. 6.7** Clustered (gray), exact (black), first estimation (red), and second estimation (green) of the mode shapes (color figure online)

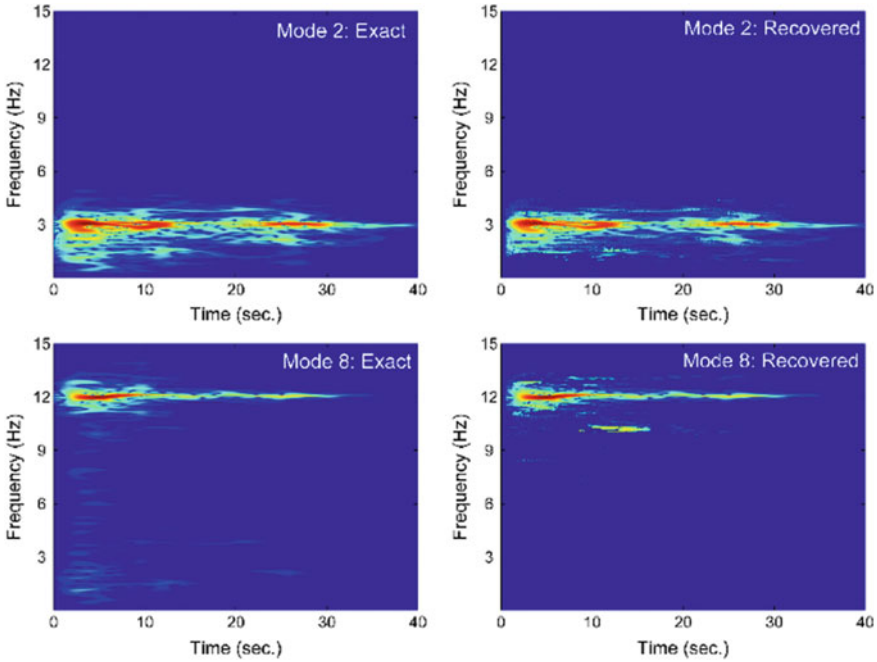


**Fig. 6.8** Comparison between the auto-TFDs of the exact and the recovered modal coordinates

position (PARAFAC) [49] to decompose the third-order tensor constructed using STFD matrices selected at SATFPs to identify the mode shapes and modal coordinates' TFDs [50]. The method—dubbed as the eXtended BMID (XB MID)—is able to handle both over-determined and underdetermined cases efficiently. The distinct decomposition procedure as well as the original BMID method are briefly described here.

First, the STFD matrices at selected SATFPs are stacked together to construct a third-order tensor as  $[\tilde{\mathbf{D}}_{\ddot{x}'}]_{ijk} = [\mathbf{D}_{\ddot{x}'\ddot{x}'}(t_k, f_k)]_{ij}$  where  $i, j = 1, \dots, n_r$  and  $k = 1, \dots, n_K$ , where  $n_K$  is the total number of SATFPs. Then, a new matrix is defined as  $[\mathbf{D}_{\ddot{q}}]_{kr} = [\mathbf{D}_{\ddot{q}\ddot{q}}(t_k, f_k)]_{rr}$  where  $r = 1, \dots, n_m$ . Per Eq. (6.5), each element of  $[\tilde{\mathbf{D}}_{\ddot{x}'}]_{ijk}$  can be expressed as

$$[\tilde{\mathbf{D}}_{\ddot{x}'}]_{ijk} = \sum_{r=1}^{n_m} [\Phi]_{ir} [\Phi]_{jr} [\mathbf{D}_{\ddot{q}}]_{kr}. \quad (6.27)$$

The equation above implies that  $\tilde{\mathbf{D}}_{\ddot{x}'}$  can be decomposed into  $n_m$  rank-one tensors and that the mode shape matrix can be identified in this manner. To do so, the tensor  $\tilde{\mathbf{D}}_{\ddot{x}'}$  can be expressed as a generalized STFD matrix as  $[\mathbf{D}_{\ddot{x}'}]_{(i-1)n_r+j,k} = [\tilde{\mathbf{D}}_{\ddot{x}'}]_{ijk}$ . The

Khatri-Rao representation of this  $n_r^2 \times n_K$  matrix, which is equivalent to Eq. (6.27) is given as

$$\underline{\mathbf{D}}_{\dot{\mathbf{x}}_r} = (\Phi \odot \Phi) \mathbf{D}_{\dot{\mathbf{q}}}^T \quad (6.28)$$

where  $\odot$  is the Khatri-Rao product operator. The SVD of  $\underline{\mathbf{D}}_{\dot{\mathbf{x}}_r}$  is simply,

$$\underline{\mathbf{D}}_{\dot{\mathbf{x}}_r} \approx \mathbf{U} \mathbf{\Delta} \mathbf{V}^T \quad (6.29)$$

where  $\mathbf{U}$  and  $\mathbf{V}$  are  $n_r^2 \times n_m$  and  $n_K \times n_m$  column-wise, respectively;  $\mathbf{\Delta}$  is an  $n_m \times n_m$  positive-definite diagonal matrix. Equations (6.28) and (6.29) imply that there exist an  $n_m \times n_m$  non-singular unknown matrix  $\mathbf{F}$  such that

$$\Phi \odot \Phi = \mathbf{U} \mathbf{\Delta} \mathbf{F}, \quad (6.30)$$

$$\mathbf{D}_{\dot{\mathbf{q}}} = \mathbf{V} \mathbf{F}^{-T}. \quad (6.31)$$

By computing the matrix  $\mathbf{F}$ —whose details can be found in the paper by [50]—, the mode shape matrix  $\Phi$  and modal coordinates' TFDs at selected SATFPs,  $\mathbf{D}_{\dot{\mathbf{q}}}$ , can be easily estimated, while the approach presented in the last section could be also used to recover the modal coordinates' TFDs at all time-frequency points.

The XBMID is the most complete version of the BMID and has been verified, validated, and applied to various real-life case studies (see, for example, [25, 51, 52]). Figure 6.9 shows a scaled 10-story structure, which was constructed and tested at Iran's International Institute of Earthquake Engineering and Seismology (IIIES). Data from those tests are used to validate the XBMID technique. The structure was excited under various types of ground motions (Fig. 6.10) and the identified mode shapes are verified through comparing results with those identified by an IO method, ERA/OKID [18]. As seen in Table 6.4, MAC indices for almost all modes and all shake table tests are close to 1.

### 6.2.1.7 Non-classical Damping

As mentioned at the beginning of this chapter, non-classical damping is an attribute that is encountered in the identification of SSI systems, due to the concentrated damping source provided by the soil-foundation system that the superstructure interacts with. The studies on modal identification in the presence of non-classical damping are quite limited (see, for example, [53, 54]). This is primarily due to inherent complexities of the problem. Specifically, imperfections and measurement noise could themselves result in complex-valued mode shapes; and modal damping ratios are always highly uncertain due to their low observability in recorded data even for systems with classical damping. Nevertheless, the authors have developed a special version of XBMID that is able to identify modal properties of a system with non-



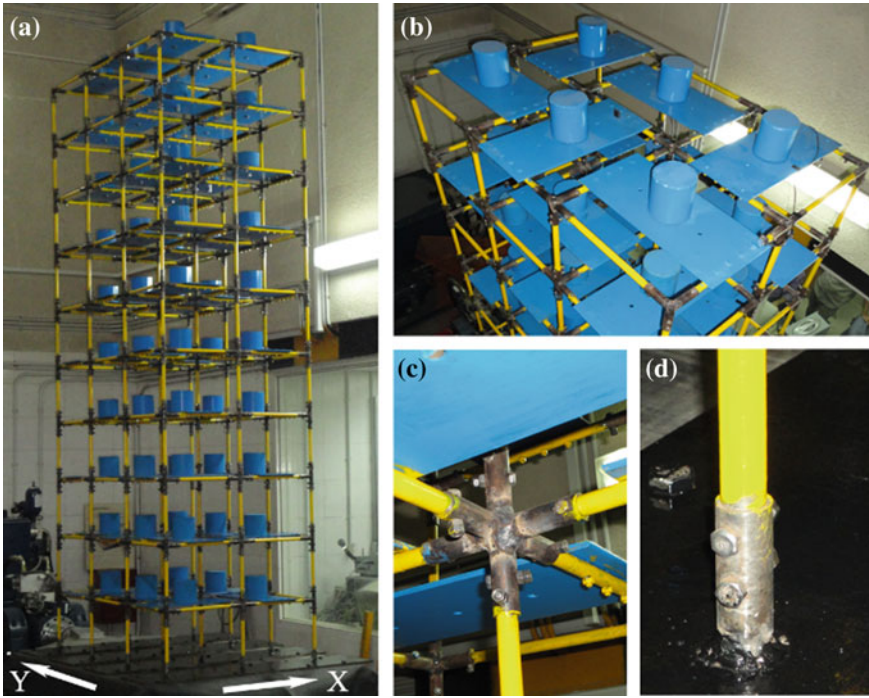


**Fig. 6.9** a IIEES test structure; b distribution of additional masses; c beam-column; d column-base connection

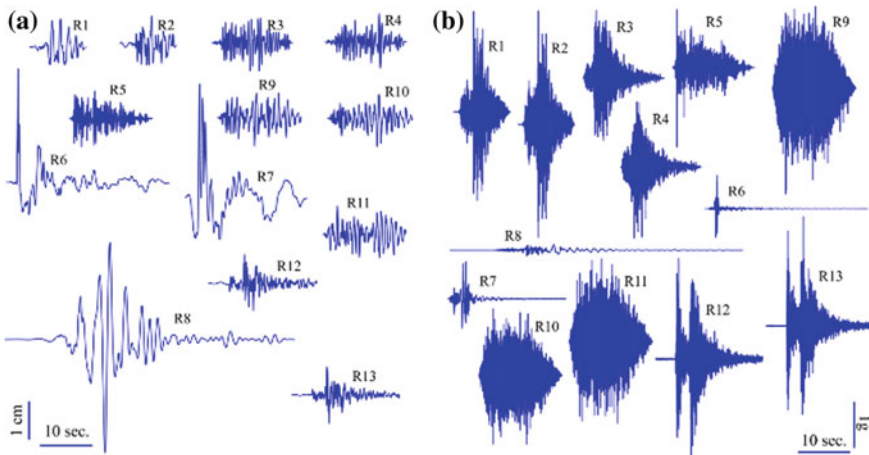


**Fig. 6.10** a Displacement and b acceleration time histories of the ground motions



**Table 6.4** MAC indices between the identified mode shapes from XB MID and ERA/OKID

Record no. →	1	2	3	4	5	6	7	8	9	10	11	12	13
Mode no. 1	0.95	1.00	1.00	1.00	0.97	0.95	0.94	0.92	0.99	0.99	0.98	1.00	1.00
2	NA *	0.95	0.93	0.98	0.93	NA	NA	0.98	0.93	0.93	0.94	1.00	0.96
3	0.91	0.99	0.96	0.90	0.98	0.91	0.96	1.00	0.97	0.96	0.98	1.00	0.98
4	0.78	1.00	1.00	1.00	0.99	0.98	NA	1.00	0.99	1.00	1.00	1.00	0.98
5	NA	0.93	0.96	0.87	0.99	0.98	0.90	0.85	0.99	0.99	0.95	0.85	1.00
6	0.95	0.91	0.98	0.99	0.94	0.71	0.80	1.00	0.98	0.99	0.99	0.86	0.99
7	0.83	0.96	0.99	0.98	0.99	0.76	0.97	0.95	1.00	0.98	0.95	1.00	1.00
8	0.99	0.99	0.95	1.00	0.99	NA	0.98	0.99	1.00	0.99	0.95	0.99	0.99
9	0.98	0.97	0.99	0.96	0.94	na	na/NA	0.98	1.00	0.98	1.00	1.00	0.99
10	na**	1.00	0.94	0.92	0.69	na/NA	na	0.97	1.00	0.99	0.98	1.00	0.97

\*NA: Not identified by ERA/OKID

\*\*na: Not identified by XB MID method

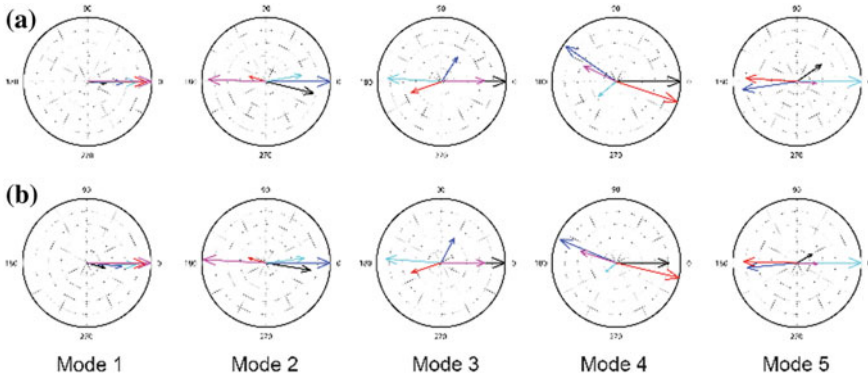


**Fig. 6.11** Comparison between exact (a) and identified (b) mode shapes

classical damping from earthquake-induced responses [55]. The main innovation of this improvement is described in what follows.

According to the modal superposition rule, it can be shown that the absolute acceleration of a system with non-classical damping can be expressed as

$$\ddot{\mathbf{x}}^t(t) = \Phi \mathbf{q}(t) + \Phi^* \mathbf{q}^*(t) \tag{6.32}$$

where  $\Phi = [\phi_1 \dots \phi_{n_m}]$  and  $\ddot{\mathbf{q}}(t) = \ddot{\mathbf{q}}_R(t) + i\ddot{\mathbf{q}}_I(t) = [q_1(t) \dots q_{n_m}(t)]^T$  are the complex-valued mode shape matrix and the modal coordinate vector, respectively. The redundant complex-conjugate term can be eliminated by converting the acceleration response signals to their analytic forms, because modal coordinates are themselves analytic signals. That is,

$$\tilde{\mathbf{x}}^t(t) = \Phi \ddot{\mathbf{q}}(t). \tag{6.33}$$

Now, by calculating the STFD of both sides of the equation above, we have

$$\mathbf{D}_{\tilde{\mathbf{x}}^t \tilde{\mathbf{x}}^t}(t, f) = \Phi \mathbf{D}_{\ddot{\mathbf{q}} \ddot{\mathbf{q}}}(t, f) \Phi^H, \tag{6.34}$$

which is similar to Eq. (6.5), except for the fact that the conventional matrix transpose is replaced with a Hermitian Transpose. So, a complex-valued non-unitary Joint Approximate Diagonalization (JAD) (e.g., [56]) can be employed to identify the mode shapes from  $\mathbf{D}_{\tilde{\mathbf{x}}^t \tilde{\mathbf{x}}^t}(t, f)$  at the SATFPs. To verify the proposed method, mode shapes of a 5-story shear-building model that has a non-classical damping source are identified from its responses simulated using ground accelerations. The identified complex-valued mode shapes are displayed in Fig. 6.11 via polar plots along with their exact (analytically computed) counterparts. As seen, the method is able to successfully identify the system’s complex-valued mode shapes.

## 6.2.2 Model-Based Identification Techniques

Although BMID techniques were shown to be successful in the identification of systems for which input excitation is not available, especially SSI systems, they suffer from various critical issues. First, they are modal methods, and thus, they are limited to linear-elastic systems, whereas soil behavior is typically quite nonlinear even under weak excitations. Second, the performance of BMID techniques (generally all modal identification methods) is highly sensitive to the number of sensors. Model-based identification techniques are appealing alternatives to modal methods, which are especially fruitful for SSI systems. Typically models serve as implicit sources of information and enable reduction of the number of sensors. Model-based techniques, by definition, employ model updating techniques (see, for example, [57]). That is, a preliminary numerical model of a structure/system is created and manipulated such that it exhibits a close response to what is measured in real-life.

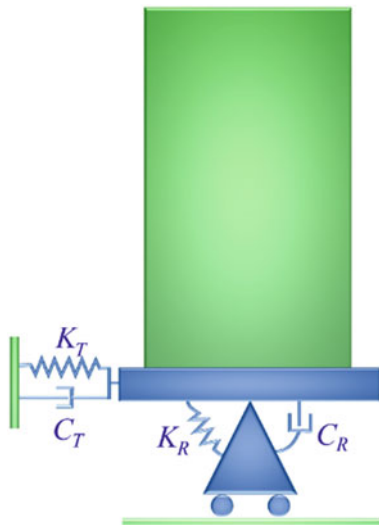
While the identified mode shapes and natural frequencies (i.e., frequency domain data) can be used as input in model updating studies (e.g., [25, 58–60]), the essential benefit of model-based methods in the identification of SSI systems is their ability to work entirely in the time-domain, which enables direct consideration of nonlinear behavior.

### 6.2.2.1 Simple Models

SSI systems are composed of two substructures, (i) the superstructure, and (ii) the soil-foundation system. The former is manmade, so it could be analytically or numerically modeled with acceptable accuracy, while the latter is not easily modeled due to the complexities of soil nonlinearities and SSI phenomena. As such, and due to the fact that SSI is usually significant in lower vibration modes [26], one idea that has been employed in prior studies is to represent the superstructure with a simple model that has only a few parameters (e.g., [61]), so that the more-complex soil-foundation system and the unknown FIMs can be identified from available data. For example, a Timoshenko beam model has been used to represent the superstructure, which exhibits both shear and flexural deformations as well as rotary inertia (e.g., see [62]). The authors have developed a technique along this line for identification of SSI systems [63], which is summarized next.

Consider a Timoshenko beam on a sway-rocking soil-foundation system as shown in Fig. 6.12, and assume that we have measured the response of the system at three locations, which incidentally is the most common building instrumentation scenario in the US (foundation sway, and horizontal motion at the mid-height, and roof levels). The Fourier amplitude (denoted by an overbar) of the absolute acceleration of this model at the normalized height  $\tilde{z}$  under a horizontal FIM is given by

**Fig. 6.12** Timoshenko beam model of a soil-structure system



$$\bar{x}^t(\tilde{z}, \omega) = \left[ \sum_{j=1}^{n_m} W_j(\tilde{z}) \frac{L_j^*}{m_j^*} H_j(\omega) + 1 \right] \bar{u}_g(\omega) \tag{6.35}$$

where  $W_j(\tilde{z})$  is the  $j$ -th translational mode shape, and  $\bar{u}_g(\omega)$  is the Fourier amplitude of the horizontal FIM.  $L_j^*$  and  $m_j^*$  are respectively the generalized influence factor and mass, and  $H_j(\omega)$  is

$$H_j(\omega) = \frac{-\omega^2}{\omega_j^2 - \omega^2 + 2i\xi_j\omega_j\omega} \tag{6.36}$$

where  $\xi_j$  and  $\omega_j$  are  $j$ th flexible-base mode's damping ratio and natural frequency, respectively. Consequently, the absolute acceleration of the mid-height and the roof levels can be predicted by the foundation sway response signal  $\bar{x}_b^t(\omega)$  as

$$\bar{x}^t(\tilde{z}, \omega) = \frac{\left[ \sum_{j=1}^n W_j(\tilde{z}) \frac{L_j^*}{m_j^*} H_j(\omega) + 1 \right]}{\left[ \sum_{j=1}^n W_j(0) \frac{L_j^*}{m_j^*} H_j(\omega) + 1 \right]} \bar{x}_b^t(\omega). \tag{6.37}$$

So, all unknown parameters of both the superstructure and the soil-foundation system can be identified by minimizing the misfit between the predicted and recorded mid-height and roof levels responses in a least-squares sense without the need to measure/record FIMs. The updating parameters are those controlling the behavior of the Timoshenko beam  $s = \sqrt{EI/GA_s L^2}$  and  $\bar{b} = \rho AL^4/EI$ , parameters of the soil-foundation system  $k_R = K_R L/EI$  and  $k_T = K_T L/GA_s$ , and the modal damping ratios  $\xi_1, \dots, \xi_{n_m}$ , where  $L$  denotes the building's height,  $\rho$  is the mass

**Fig. 6.13** The Millikan Library



density,  $A$  is the cross-sectional area,  $I$  is the area moment of inertia, and  $E$  and  $G$  are the Young's and shear moduli, respectively.  $A_s = kA$  is the effective cross-sectional area of the superstructure model with the correction factor being  $k = 0.85$  for rectangular sections.  $K_T$  and  $K_R$  (see, Fig. 6.12) are the sway and rocking soil-foundation stiffnesses.

To verify the proposed identification approach, we use real earthquake data recorded on the Millikan Library (Fig. 6.13) along the North-South (NS) direction during the 2002 Yorba Linda earthquake. Figure 6.14a presents a comparison of the recorded signals at mid-height and roof levels and those predicted by the identified model (Fig. 6.12). As seen, the model is successful in representing a real-life soil-structure system. The blind prediction of other floors' responses that are not used in the identification process, is also very accurate, as seen in Fig. 6.14b.

### 6.2.2.2 Finite Element Models

Thanks to ever-advancing computational capabilities, Finite Element (FE) analyses of complex large-scale structures are becoming routine tasks. This is crucial for identification purposes, because a given model has to be analyzed many times during iterations of model-based identification procedures. Time-domain output-only FE model updating methods that are based on Bayesian filtering techniques have attracted significant attention recently due to their superior performances (see, for example, [64, 65]). In these techniques, the prior probability distributions of unknown parameters of an FE model, along with the unknown input excitations are updated iteratively through information collected through the measurements (see, Fig. 6.15). The probabilistic framework of these methods makes the possibility to

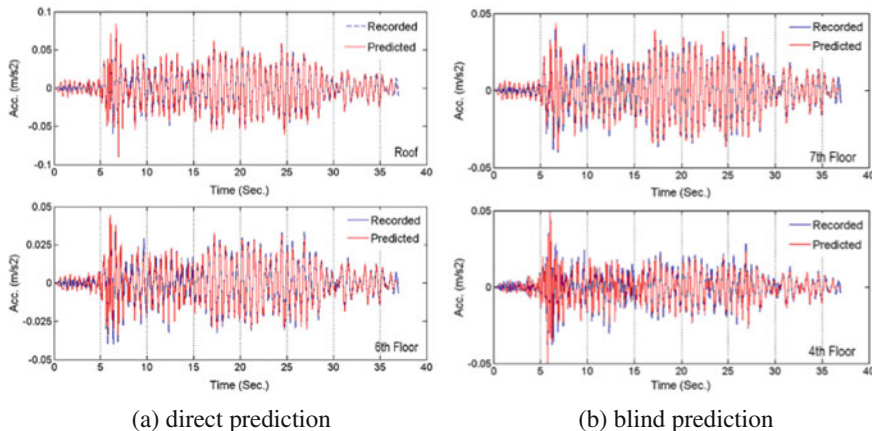


**Fig. 6.14** Comparison between recorded (blue) and predicted (red) absolute acceleration (color figure online)

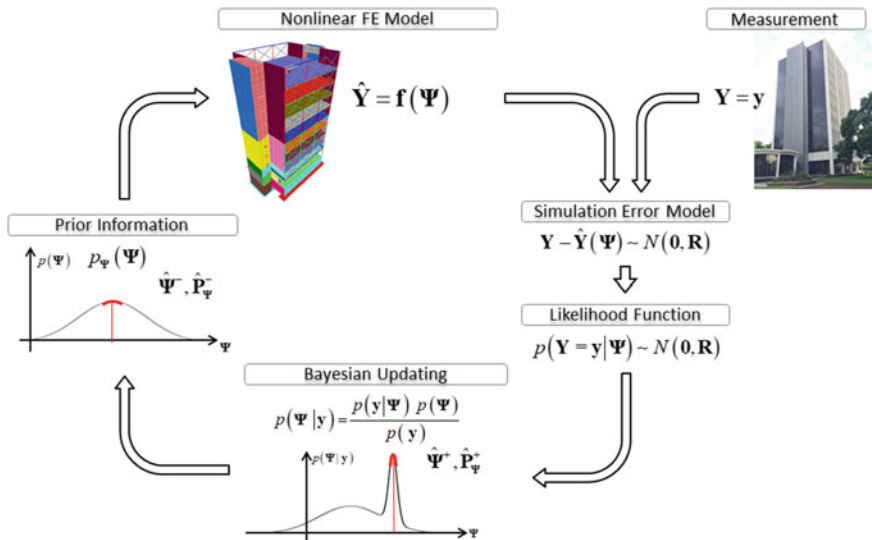


**Fig. 6.15** Schematic presentation of the sequential Bayesian FE model updating method [66]

quantify uncertainties associated with the estimation. The details of these methods can be found in the mentioned above references. Herein, we present a few practical applications.

The first example shows the application of the method to the FE model of the Millikan Library [25] and Yorba Linda earthquake [67]. Figure 6.16 displays the predicted (using the identified model parameters and FIM) versus measured responses at two floors. As seen, the predictions are quite accurate.

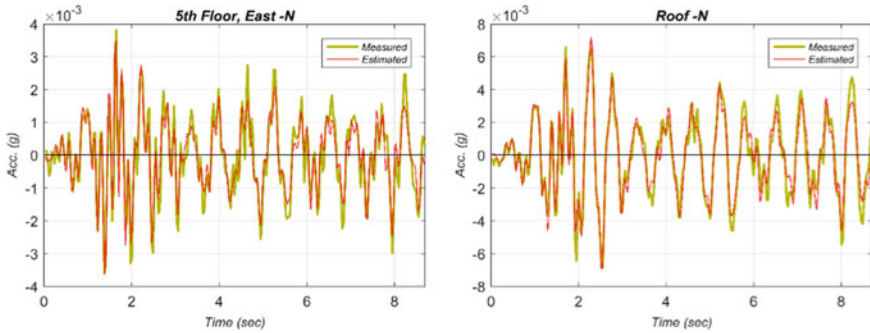


**Fig. 6.16** Comparison between recorded (green) and predicted (red) absolute acceleration responses [67] (color figure online)

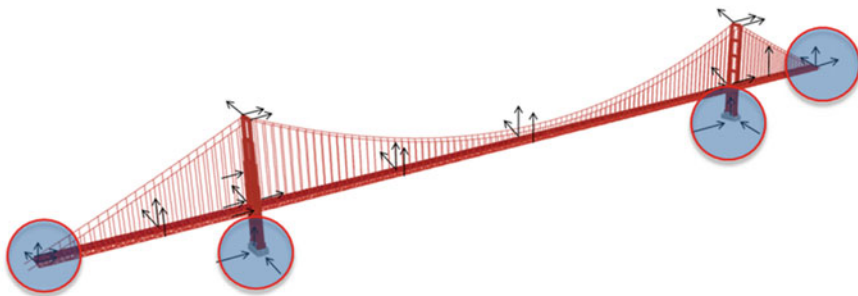


**Fig. 6.17** FE model of the Golden Gate Bridge (GGB) with available instrumentation channels indicated by arrows (circles indicate channels considered as input excitations)

The next example is the application of the method to a very large-scale problem involving the Golden Gate Bridge (GGB) under multiple unknown FIMs (Fig. 6.17). We simulated the response of this model using data recorded at the foundation levels (sensors are marked with circles in figure) during the 2014 South Napa earthquake, and subsequently identified various unknown parameters of the model as well as the input excitations. Figure 6.18 displays the exact and the identified FIMs at the base of the two main towers (South tower: CH31, 32, 33; North tower: CH16, 17, 18). The results displayed in this figure indicate that the method works very well. However, it should be kept in mind that these methods are very expensive computationally, because the unknown FIMs are identified along with the system’s parameters, which makes the computational burden extremely high, especially because the superstructure’s geometric nonlinearities were considered.

If the system’s parameters are the main interest, then it is more favorable to utilize an output-only FE model updating method wherein the unknown FIMs do not have to be identified simultaneously, in order to keep the computational expenses low. This can be done using a Cross-Relation (CR) technique [68] provided that we have at least two neighboring instrumented buildings (Fig. 6.19). It is easy to show that following

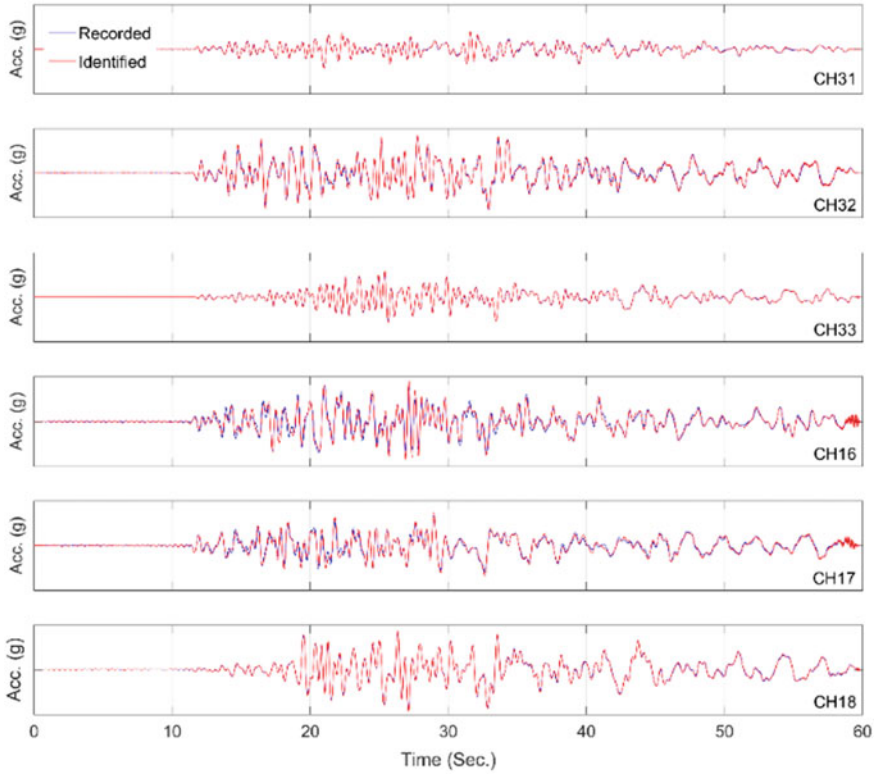


**Fig. 6.18** Comparison between the exact and the identified FIMs for GGB

cross-relation can be written between measured responses (e.g., those recorded at the roof levels of the two buildings)

$$\left\{ y_1^{\sin \alpha \ddot{x}_1} + x_1^{\cos \alpha \ddot{y}_1} \right\} * h_2 - \left\{ y_2^{\sin \beta \ddot{x}_2} + x_2^{\cos \beta \ddot{y}_2} \right\} * h_1 \approx 0, \quad (6.38)$$

$$\left\{ y_1^{\cos \alpha \ddot{x}_1} + x_1^{-\sin \alpha \ddot{y}_1} \right\} * h_2 - \left\{ y_2^{\cos \beta \ddot{x}_2} + x_2^{-\sin \beta \ddot{y}_2} \right\} * h_1 \approx 0, \quad (6.39)$$

where, for example,  $y_1^{\sin \alpha \ddot{x}_1}$  stands for the response of Building 1 in its local  $y$ -direction under the input excitation  $\sin \alpha \ddot{x}_1$ , in which  $\ddot{x}_1$ ,  $\ddot{y}_1$ ,  $\ddot{x}_2$ , and  $\ddot{y}_2$  are the recorded responses in local  $x$ - and  $y$ -directions of Buildings 1 and 2, respectively. Also,  $h_1 = h_1^x * h_1^y$  and  $h_2 = h_2^x * h_2^y$  where  $h_i^j$  is the impulse response function of Building  $i$  along the  $j$ -direction, and  $*$  denotes a linear convolution. The approximate equal sign is used in the equation above to indicate that there is measurement noise. Based on the equations above, we can identify the parameters of two buildings' FE models by minimizing the left-hand sides of Eqs. (6.38) and (6.39).



**Fig. 6.19** Two nearby instrumented buildings under a bidirectional seismic excitation

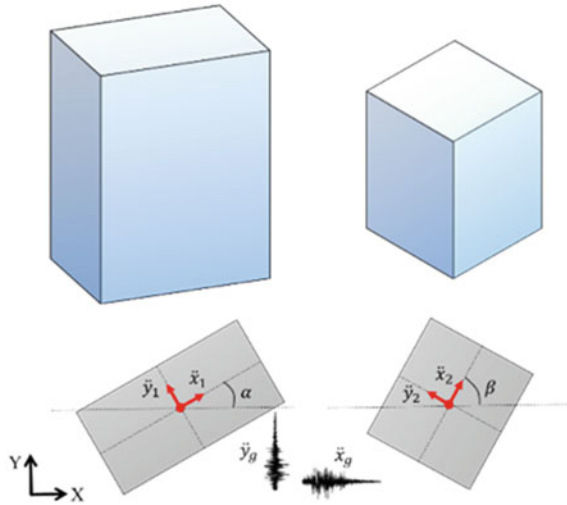


**Table 6.5** Identified mean errors and COVs for the cross-relation method verification study

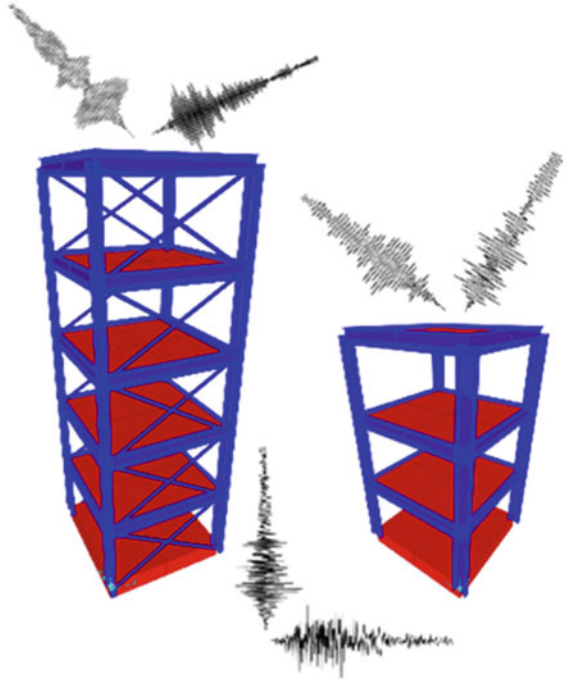
Parameters	$K_y(1)$	$K_x(1)$	$K_y(2)$	$K_x(2)$	$\alpha(1)$	$\beta(1)$	$\alpha(2)$	$\beta(2)$
Final error (%)	0.02	3.65	0.15	0.17	1.61	–	1.85	–
Final COV (%)	0.06	1.75	0.02	0.06	0.48	17.59	0.11	12.74

Figure 6.20 displays the results of a verification study on two buildings whose responses are numerically simulated under bi-directional ground accelerations and polluted by random noise. The stiffnesses of the soil-foundation rocking springs at the bottom of buildings along with the Rayleigh damping ( $\alpha\mathbf{M} + \beta\mathbf{K}$ ) coefficients are attempted to be identified through the proposed cross-relation approach. Table 6.5 presents the final relative errors in the identified values along with their Coefficients-of-Variation (COVs). As seen, while we assumed an initial 50% error in the system parameters at the beginning of the identification, the method yields negligible final errors. Also, the COVs indicate that the estimated values are highly reliable.

### 6.3 Conclusions

This chapter reviewed the most recent developments in the identification of soil-structure systems from seismic responses. This identification task is a challenging one due to the typically short length of recorded seismic data, the non-stationary nature of input excitations, and the potential nonlinearities of soil-structure systems. More importantly, soil-structure interaction renders it virtually impossible to directly measure the earthquake input motions. So, identification tasks must be carried out

**Fig. 6.20** Verification study for the cross-relation method



in an output-only mode, but the classical output-only identification techniques are typically based on specific statistical assumptions regarding the unknown external forces (e.g., white with zero-mean), which are no longer valid for the seismic case. Through work spanning the past decade—by the authors, their collaborators, as well as other colleagues—various new methods of system identification have been devised to tackle these soil-structure identification problems. Within the category of modal methods, a particularly fruitful class of methods comprised Blind Modal Identification (BMID) techniques, which were reviewed from their genesis to their most recent versions. Model-based techniques were also presented through which various limitations of BMID methods are removed or relaxed, albeit by increasing the computational costs and the labor involved in the development of initial models.

**Acknowledgements** The authors would like to acknowledge M. Ali Ghannad, Mehmet Celebi, Fariborz Nateghi, Anoosh Shamsabadi, Robert Nigbor, Hamed Ebrahimian, Mojtaba Mahsuli, and Nima Shirzad for their contributions to the studies reviewed in this chapter. The authors also acknowledge California Department of Transportation (Caltrans) and California Geological Survey (CGS), which provided financial support for research whose results were presented in this chapter.

## References

1. Jennings PC, Kuroiwa JH (1968) Vibration and soil-structure interaction tests of a nine-story reinforced concrete building. *Bull Seismol Soc Am* 58(3):891–916
2. Richart FE Jr. (1975) Some effects of dynamic soil properties on soil-structure interaction. *J Geotech Geoenvironmental Eng* 101(ASCE# 11764 Proceeding)
3. Wolf JP (1976) Soil-structure interaction with separation of base mat from soil (lifting-off). *Nucl Eng Des* 38(2):357–384
4. Wolf JP, Deeks AJ (2004) *Foundation vibration analysis: a strength of materials approach*. Butterworth-Heinemann
5. Luco JE, Mita A (1987) Response of circular foundation to spatially random ground motion. *J Eng Mech* 113(1):1–15
6. Luco JE, Wong HL (1986) Response of a rigid foundation to a spatially random ground motion. *Earthq Eng Struct Dyn* 14(6):891–908
7. Veletsos AS, Prasad AM, Wu WH (1997) Transfer functions for rigid rectangular foundations. *Earthq Eng Struct Dyn* 26(1):5–17
8. Apsel RJ, Luco JE (1976) Torsional response of rigid embedded foundation. *J Eng Mech Div* 102(6):957–970
9. Mita A, Luco JE (1989) Impedance functions and input motions for embedded square foundations. *J Geotech Eng* 115(4):491–503
10. Pais AL, Kausel E (1989) On rigid foundations subjected to seismic waves. *Earthq Eng Struct Dyn* 18(4):475–489
11. Mahsuli M, Ghannad MA (2009) The effect of foundation embedment on inelastic response of structures. *Earthq Eng Struct Dyn* 38(4):423–437
12. Rizos DC, Wang Z (2002) Coupled BEM-FEM solutions for direct time domain soil-structure interaction analysis. *Eng Anal Bound Elem* 26(10):877–888
13. Lysmer J, Kuhlemeyer RL (1969) Finite dynamic model for infinite media. *J Eng Mech Div* 95(4):859–878
14. Juang JN, Pappa RS (1985) An eigensystem realization algorithm for modal parameter identification and model reduction. *J Guid Control Dyn* 8(5):620–627
15. Van Overschee P, De Moor B (1993) Subspace algorithms for the stochastic identification problem. *Automatica* 29(3):649–660
16. Brincker R, Zhang L, Andersen P (2001) Modal identification of output-only systems using frequency domain decomposition. *Smart Mater Struct* 10(3):441–445
17. Pioldi F, Rizzi E (2018) Assessment of frequency versus time domain enhanced technique for response-only modal dynamic identification under seismic excitation. *Bull Earthq Eng* 16(3):1547–1570
18. Lus H, Betti R, Longman RW (1999) Identification of linear structural systems using earthquake-induced vibration data. *Earthq Eng Struct Dyn* 28(11):1449–1467
19. Stewart JP, Fenves GL, Seed RB (1999) Seismic soil-structure interaction in buildings. I: analytical methods. *J Geotech Geoenvironmental Eng* 125(1):26–37
20. Todorovska MI (2009) Soil-structure system identification of Millikan Library North-South response during four earthquakes (1970–2002): what caused the observed wandering of the system frequencies? *Bull Seismol Soc Am* 99(2A):626–635
21. Veletsos AS, Ventura CE (1986) Modal analysis of non-classically damped linear systems. *Earthq Eng Struct Dyn* 14(2):217–243
22. Stewart JP, Seed RB, Fenves GL (1998) Empirical evaluation of inertial soil-structure interaction effects. Pacific Earthquake Engineering Research Center
23. Kuroiwa J (1967) Vibration tests of a multistory building. California Institute of Technology
24. Keightley WO (1963) Vibration tests of structures. Technical report: Caltech EERL.1963.001
25. Ghahari SF, Abazarsa F, Avci O, Çelebi M, Taciroglu E (2016) Blind identification of the Millikan Library from earthquake data considering soil-structure interaction. *Struct Control Heal Monit* 23(4):684–706

26. Luco JE (1980) Soil-structure interaction and identification of structural models. In: Proceedings of 2nd ASCE conference on civil engineering and nuclear power, vol 2, pp 10–11
27. Safak E (1995) Detection and identification of soil-structure interaction in buildings from vibration recordings. *J Struct Eng* 121(5):899–906
28. Stewart JP, Fenves GL (1998) System identification for evaluating soil-structure interaction effects in buildings from strong motion recordings. *Earthq Eng Struct Dyn* 27(8):869–885
29. Safak E (2009) System identification for soil—structure interaction. *Encycl Struct Heal Monit*
30. Stewart JP, Stewart AF (1997) Analysis of soil-structure interaction effects on building response from earthquake strong motion recordings at 58 sites, vol 97, no 1. Earthquake Engineering Research Center
31. Ghahari SF, Abazarsa F, Ghannad MA, Taciroglu E (2013) Response-only modal identification of structures using strong motion data. *Earthq Eng Struct Dyn* 42(8)
32. Belouchrani A, Amin MG (1998) Blind source separation based on time-frequency signal representations. *IEEE Trans Signal Process* 46(11):2888–2897
33. Chopra AK (1995) Dynamics of structures, vol 3. Prentice Hall, New Jersey
34. Boashash B (2003) Time frequency signal analysis and processing: a comprehensive reference
35. Flandrin P (1984) Some features of time-frequency representations of multicomponent signals. *Proc IEEE Int Conf Acoust Speech Signal Process* 3(1):41B.4.1–41B.4.4
36. Mathworks (2014) MATLAB the language of technical computing
37. Flandrin P (1999) Time-frequency/time-scale analysis. *Wavelet Anal Appl* 10:49–182
38. Cardoso J-F, Souloumiac A (1996) Jacobi angles for simultaneous diagonalization. *SIAM J Matrix Anal Appl* 17(1):161–164
39. Nguyen L-T, Belouchrani A, Abed-Meraim K, Boashash B (2005) Separating more sources than sensors using time-frequency distributions. *EURASIP J Appl Signal Process* 17:2005
40. Taciroglu E, Abazarsa F, Ghahari SF (2012) Response-only identification of torsionally coupled buildings using strong motion data. In: 9th international conference on urban earthquake engineering/4th Asia conference on earthquake engineering
41. Chopra AK, la Llera JC (1996) Accidental and natural torsion in earthquake response and design of buildings. In: Eleventh world conference on earthquake engineering
42. Ventura CE, Mirza K (2005) Model calibration of a 3-story steel frame building using earthquake records. In: IMAC-XXIII, conference & exposition on structural dynamics
43. Ghahari SF, Ghannad MA, Norman J, Crewe A, Abazarsa F, Taciroglu E (2013) Considering wave passage effects in blind identification of long-span bridges. In: Conference proceedings of the society for experimental mechanics series, vol 5
44. Norman JAP, Crewe AJ (2008) Development and control of a novel test rig for performing multiple support testing of structures. In: Proceedings of the 14th world conference on earthquake engineering, Beijing, paper, no. 2–2, p 51
45. Ghahari SF, Abazarsa F, Ghannad MA, Celebi M, Taciroglu E (2014) Blind modal identification of structures from spatially sparse seismic response signals. *Struct Control Heal Monit* 21(5)
46. Giulieri L, Ghennioui H, Thirion-Moreau N, Moreau E (2005) Nonorthogonal joint diagonalization of spatial quadratic time-frequency matrices for source separation. *IEEE Signal Process Lett* 12(5):415–418
47. Aïssa-El-Bey A, Linh-Trung N, Abed-Meraim K, Belouchrani A, Grenier Y (2007) Underdetermined blind separation of nondisjoint sources in the time-frequency domain. *IEEE Trans Signal Process* 55(3):897–907
48. Abazarsa F, Ghahari SF, Nateghi F, Taciroglu E (2013) Response-only modal identification of structures using limited sensors. *Struct Control Heal Monit* 20(6)
49. De Lathauwer L, Castaing J (2008) Blind identification of underdetermined mixtures by simultaneous matrix diagonalization. *IEEE Trans Signal Process* 56(3):1096–1105
50. Abazarsa F, Nateghi F, Ghahari SF, Taciroglu E (2016) Extended blind modal identification technique for nonstationary excitations and its verification and validation. *J Eng Mech* 142(2):04015078
51. Çelebi M, Kashima T, Ghahari SF, Abazarsa F, Taciroglu E (2016) Responses of a tall building with US code-type instrumentation in Tokyo, Japan, to events before, during, and after the Tohoku earthquake of 11 March 2011. *Earthq Spectra* 32(1):497–522

52. Taciroglu E, Shamsabadi A, Abazarsa F, Nigbor RL, Ghahari SF (2014) Comparative study of model predictions and data from Caltrans/CSMIP bridge instrumentation program: a case study on the Eureka-Samoa channel bridge
53. Ghahari SF, Ghannad MA, Taciroglu E (2013) Blind identification of soil-structure systems. *Soil Dyn Earthq Eng* 45
54. Abazarsa F, Nateghi F, Ghahari SF, Taciroglu E (2013) Blind modal identification of non-classically damped systems from free or ambient vibration records. *Earthq Spectra* 29(4)
55. Ghahari SF, Abazarsa F, Taciroglu E (2016) Blind modal identification of non-classically damped structures under non-stationary excitations. *Struct Control Heal Monit*
56. Maurandi V, Moreau E (2014) A decoupled jacobi-like algorithm for non-unitary joint diagonalization of complex-valued matrices. *IEEE Signal Process Lett* 21(12):1453–1456
57. Friswell MI, Mottershead JE (1995) Finite element model updating in structural dynamics, vol 38
58. Taciroglu E, Ghahari SF, Abazarsa F (2017) Efficient model updating of a multi-story frame and its foundation stiffness from earthquake records using a Timoshenko beam model. *Soil Dyn Earthq Eng* 92
59. Shirzad-Ghaleroudkhani N, Mahsuli M, Ghahari SF, Taciroglu E (2017) Bayesian identification of soil-foundation stiffness of building structures. *Struct Control Heal Monit*
60. Taciroglu E, Çelebi M, Ghahari SF, Abazarsa F (2016) An investigation of soil-structure interaction effects observed at the MIT green building. *Earthq Spectra* 32(4)
61. Miranda E, Taghavi S (2005) Approximate floor acceleration demands in multistory buildings. I: formulation. *J Struct Eng* 131(2):203–211
62. Cheng MH, Heaton TH (2015) Simulating building motions using the ratios of its natural frequencies and a Timoshenko beam model. *Earthq Spectra* 31(1):403–420
63. Taciroglu E, Ghahari SF (2017) Identification of soil-foundation dynamic stiffness from seismic response signals, no. SP 316. American Concrete Institute, ACI Special Publication
64. Astroza R, Ebrahimian H, Li Y, Conte JP (2017) Bayesian nonlinear structural FE model and seismic input identification for damage assessment of civil structures. *Mech Syst Signal Process* 93:661–687
65. Ebrahimian H, Astroza R, Conte JP, Papadimitriou C (2018) Bayesian optimal estimation for output-only nonlinear system and damage identification of civil structures. *Struct Control Heal Monit*
66. Ebrahimian H, Ghahari SF, Asimaki D, Taciroglu E (2018) A nonlinear model inversion to estimate dynamic soil stiffness of building structures
67. Ebrahimian H, Ghahari SF, Asimaki D, Taciroglu E (2018) A nonlinear model inversion to estimate dynamic soil stiffness of building structures, GSP 292. *Geotechnical Special Publication*
68. Xu G, Liu H, Tong L, Kailath T (1995) A least-squares approach to blind channel identification. *IEEE Trans Signal Process* 43(12):2982–2993